General Disclaimer

One or more of the Following Statements may affect this Document

- This document has been reproduced from the best copy furnished by the organizational source. It is being released in the interest of making available as much information as possible.

- This document may contain data, which exceeds the sheet parameters. It was furnished in this condition by the organizational source and is the best copy available.

- This document may contain tone-on-tone or color graphs, charts and/or pictures, which have been reproduced in black and white.

- This document is paginated as submitted by the original source.

- Portions of this document are not fully legible due to the historical nature of some of the material. However, it is the best reproduction available from the original submission.

NATIONAL AERONAUTICS AND SPACE ADMINISTRATION

LUNAR SAMPLE ANALYSIS PROGRAM

SURFACE PROPERTIES ANALYSIS OF LUNAR SAMPLES

RETURNED BY APOLLO

Final Report for 8/1/69 - 3/15/71

Proposal No. A-13P-1720-69W-282-2Q

"Microchemical, Microphysical and Adhesive Properties of Apollo 11 and 12"

by

J. J. Grossman, J. A. Ryan, N. R. Mukherjee and M. W. Wegner

3/15/71

Principal Investigator: Jack J. Grossman

Co-Investigators: J. A. Ryan, N. R. Mukherjee, and M. W. Wegner

Final Report

Prepared under Contract No. NAS9-8082

by

McDonnell Douglas Astronautics Company--West

5301 Bolsa Avenue

Huntington Beach, California 92647

for

NATIONAL AERONAUTICS AND SPACE ADMINISTRATION
Manned Spacecraft Center
Lunar Receiving Laboratory
Houston, Texas

CONTENTS

LIST OF FIGURES

10. Microcracks at interface of olivine crystal and ilmenite inclusion (12052,43,1,1).

11. Dislocation etch pits and twin boundaries in (a) Madagascar albite, cleaved (001), and (b, c) polished lunar plagioclase (10058,40,2).

12. Fracture face of lunar sample 12052,43,1,2,1,1. After measuring the electrostatic charge distribution, the specimen is approximately 5 mm wide. Present orientation is approximately a 150° clockwise rotation from fracture position.

Microchemical, Microphysical and Adhesive Properties of Lunar Material

J. J. Grossman, J. A. Ryan, N. R. Mukherjee, and M. W. Wegner

ABSTRACT

Disruption of lunar fines observed after exposure to O_2 and N_2O but not to N_2. Vacuum formed rock surfaces may be completely inert to dry N_2 since even mosaic electrostatic charging (scale <100μm) persists as pressure is raised to one atmosphere. Both air and U.V. exposure discharge the surface. Chemical etching revealed twinning, plastic and shock deformation in some samples, adhesion due to impact melting in others, dislocations and cosmic ray tracks. The unusual electrostatic adhesion processes of lunar material are tentatively attributed solar U.V., X-ray and cosmic ray exposure due to the absence of a lunar atmosphere.

General Descriptors:

Adhesion	Surface Properties
Defect Structure	Apollo 11 and 12
Electrostatic Charging	Ultrahigh Vacuum

Specific Descriptors:

Pyroxenes	Air	Ilmenite	N_2
Plagioclase	H_2O	Olivine	O_2
Chromite	Adsorption	Exsolution	Diffusion
Twinning	Weight Gain	Solar Wind	Ultraviolet
Cosmic Rays	F-601	Dislocations	UHV Shipping
Tracks	SEM	Etch Pits	EMX

Chemical Etching	Polishing	Impact	Etching Solutions
Melting	UHV Fracture	Meteorite	Porosity
Micrometeorite	Work Function		

MICROCHEMICAL, MICROPHYSICAL AND ADHESIVE PROPERTIES OF LUNAR MATERIAL, II

J. J. Grossman, J. A. Ryan, N. R. Mukherjee, and M. W. Wegner

Space Sciences Department

McDonnell Douglas Astronautics Company--West

Huntington Beach, California 92647

SUMMARY

A vacuum pumped Apollo lunar sample 12001,118, was transported successfully from the Lunar Receiving Laboratory to the McDonnell Douglas Astronautics Company--West (MDAC-W) laboratories for gas exposure experiments. Disruption in oxygen has been observed. Etching techniques of the defect structure have been improved, and both dislocations and tracks are found simultaneously. Heavy cosmic ray tracks have been found in pyroxenes and ilmenite. Track gradients show that the (E, S, T) face of 12052,43 has been exposed to the solar wind. The net adhesion force of a UHV fractured specimen of the rock fractured was too small to be measured. Measurement of electrostatic charge distributions indicated the specimen had a net positive average charge of 10^6 charges cm^{-2}. Exposure to dry N_2 does not effect the charge density. Both air and u.v. discharge the fractured faces. The unusual electrostatic adhesion processes of lunar material are tentatively attributed to the absence of a lunar atmosphere.

INTRODUCTION

The objectives of this program are to investigate the nature and relative effectiveness of mechanisms which may produce agglomeration and disruption of lunar material, and use this information to obtain an improved understanding of solid-surface phenomena. In this paper, we summarize our results of three classes of experiments on Apollo 12 lunar material, namely the effects of exposure of a vacuum sample to various gases, the microanalysis of particles and particle interfaces, and adhesion measurements in an ultrahigh vacuum system.

Experimental Methods

Gas Exposure

Lunar soil sample 12001,118 has been kept under vacuum continuously from its collection on the lunar surface in November 1969, to its delivery to our laboratory where portions were placed in reaction tubes and the remainder replaced in the NASA vacuum pumped shipping and storage container. The sequence involved sealing the Apollo 12 returned lunar sample in an aluminum container (performed in Chamber F-201 of the Lunar Receiving Laboratory), storage until November 1970 when it was opened in F-201 and placed in a special stainless steel matchbox sample container which after transfer into the ultrahigh vacuum manipulator chamber (F-601) was finally placed into the NASA vacuum pumped shipping container. The sealed shipping container, with a pressure in the mid 10^{-8} torr range, was transported to our laboratory and connected to our ultrahigh vacuum micromanipulator and sample transfer system which was evacuated to the

low 10^{-9} torr range. The shipping/storage chamber was then opened, the matchbox moved into the micromanipulator chamber, opened, and samples transferred to the gas reaction tubes (Grossman et al. 1970). After closing the matchbox, it was returned to the vacuum pumped NASA Storage Chamber which was also closed, Fig. 1. All gas reaction cells were pinch-off vacuum-sealed, the MDAC-W chamber opened, removed and connected to the UHV gas manifold, and the gas reaction experiments started.

Experimental Results

Gas Exposure

The procedure followed was the same as for the Apollo 11 samples. To date, one sample tube containing two 2.5 mm particles, one 1 mm bonded pair and some fines smaller than 200 μm has been exposed at 300°K to successively (a) pure O_2 (impurity <5 ppm) at 0.9 torr, (b) pure H_2O at 1 and 12 torr, and (c) a mixture of O_2 + 2.8 per cent H_2O at 760 torr. After eight hours of exposure under condition (a) no perceptible change was observed. However, after eighteen hours, the bonded pair was found to be disrupted. Under each of conditions (b) and (c) several small crystals were found to be disrupted from the two 2.5 mm particles after several hours of exposure. The experiment is being continued for exposure of original UHV samples to dry N_2, organic acid and organic base.

The disrupted surfaces of the lunar soil particles (sample number 10084,93; Fig. 2(b) and (d) Grossman et al. 1970b) were examined both with a light microscope and a scanning electrom microscope (SEM). A number of stereo-photographs were taken with the SEM while viewing the samples normal to these disrupted areas.

For illustrative purposes, one photograph of a stereo pair at 90° orientation of the former and one at 30° orientation of the latter are shown in Figs. 2 and 3 in which the positions of the disrupted small crystals are shown by dotted lines. A detailed examination reveals the following: (a) each disrupted area is sufficiently porous permitting interparticle diffusion of a gas, (b) the shape of individual small crystals and protrusions on larger plate-like crystals suggests some deposition and agglomeration has taken place from a liquid spray, (c) no large scale chemical reaction is apparent, (d) signatures of material fracture which are expected to remain after disruption of strong bonding are not observed at these magnifications, and (e) the presence of small crystals are probably due to comminution and rebonding processes.

High magnification photographs, such as the one in Fig. 3, show another interesting phenomenon. Droplets and small splash particles, which were formed presumably by liquid spray, appear to be comparatively less abundant in the area where the disrupted crystal contacted the larger particle. Further evidence of such deposits are found at low magnification on the surface of the disrupted crystal (shaped like rice grain). Although this evidence suggests that some of the spray deposited material occurred while the gas disrupted crystal was attached to the larger particle, the argument is weakened by the deposition asymmetry which is within 2σ of the expected statistical variance. Prior to gas exposure, the particles were also subjected to considerable mechanical motions, such as lateral motion and roll by magnetically controlled positioners (glass-coated iron wire of about 0.5 mm diameter and 3 mm long), for manipulating the particles in the field of view of the microscope. Some of the particles which appeared bonded at first separated during

translation. A few small crystals fell off from larger particles, but the crystals shown in positions discussed relative to Figs. 2 and 3 remained in position without change of orientation. They disrupted only upon exposure to gas.

Microchemical and microphysical analysis

Two samples from Apollo 12 lunar rock 12052,43 were mounted in an epoxy resin with low vacuum to assist filling pores, vugs, and vesicles. Final polishing with 0.05 μm Al_2O_3 was critical to obtain a scratch-free, minimum relief surface. Residues which remain after etching, produced in part by the greater reactivity of the polish-damaged surface layer, were removed using suitable chemical complexing agents. The etchants, used to accommodate the different etch rates of the lunar mineral species, in decreasing etch-rate order are as follows: H_2SiF_6:HCl:Citric Acid (1:1:1); HBF_4 substituted for H_2SiF_6; HF:HCl:H_2O (1:3:8); and HF:HCl:Citric Acid (1:1:1).

The smaller section of 12052,43 designed ,2, was mounted in epoxy and oriented so that the normal to the polished surface was the body diagonal penetrating the NASA orientation cube at the corner intersection of the E, S, and T planes. An adjacent flat chip from the remaining long section, designated ,43,1,1 was also mounted in epoxy and polished, exposing the outer surface of the rock.

Sample 12052,43,2 was etched with the last three of the series of etchants, after the second polishing. There was no repolishing between the etching steps. The HBF_4:HCl:Citric Acid produced both dislocation etch figures as well as numerous randomly oriented tracks in olivine, (Fig. 4). The rectangular dislocation etch figures are characteristic of the (100) face (Maurette, 1966;

Young, 1966; Wegner and Grossman, 1969). The dislocation density is 7×10^6 cm^{-2} and the track density is 1.8×10^7 cm^{-2}. Slight etching of plagioclase laths and some glassy areas was observed.

The second etching step, using $HF:HCl:H_2O$, caused deep etching of olivine although still recognizable, and etching of the glassy matrix, plagioclase laths and skeletal crystals. Plagioclase exhibited dislocation etch pits, some polygonized dislocations, defects at twin boundaries, and tracks. Ilmenite crystals were not etched.

The last etchant produced exsolution striations in pyroxenes, and tracks in both pyroxenes and ilmenite. Cosmic ray tracks in pyroxene appeared as round dots in the light microscope (Fig. 5). Other cosmic ray tracks were found on the edges of two pyroxene crystals (Fig. 6) and on the edge of a pyroxene-ilmenite crystal interface (Fig. 7). The shape of these tracks and their distribution, similar in both pyroxene and ilmenite, are characteristic of heavy cosmic ray tracks as described by Fleischer et al. (1967). The ilmenite crystal was a border surrounding a chromium-spinel core with a composition similar to that found in 12013, 10, area 24 (Lunatic Asylum, 1970). A pyroxene crystal with an hourglass structure visible in polarized light produced dense etching striations in the outer portion (Fig. 8). EMX analysis showed higher Ca, lower Mg, and slightly less Fe and Si in the etched region as compared to the central portion. Another pyroxene crystal, which penetrated the exterior surface of the rock, provided a track density gradient 70 μm into the surface. The density gradient corresponded to that reported by Fleischer et al. (1970), but the net density was a factor of three less. This indicates that the (E, S, T) face of 12052 was exposed to the solar wind.

Dislocation etch figures and track densities varied with the crystal orientation (Condie et al. 1969; Wegner and Grossman, 1969; Barber et al. 1971). In section 12052.43,1,1, the olivine (100) and (010) surfaces (Fig. 9) were first identified by their characteristic etch pit shapes (Grossman et al. 1970a; Wegner and Grossman, 1969) and later confirmed by EMX composition analysis, Table I. Although the chemical composition of the four olivines is quite similar, their reaction with the same etchant (H_2SiF_6 complex) varied; two of the crystals were more heavily etched and acquired a brown discoloration. Both crystal orientation, most probably (001), and minor elements in the mineral which modify the crystal free energy, can change its reactivity (Belov, 1965). The specific source of the staining has not been identified.

Microcracks at interfaces of mineral species were observed by optical microscopy and scanning electron microscopy. An example of an olivine crystal with microcracks at the ilmenite inclusion in sample 12052,43,1,1 is shown in Fig. 10. Electronmicrographs of terrestrial twinned albite, cleaved and etched Fig. 11a (Grossman et al.), are compared to polished and etched twinned lunar plagioclase in 10058,40,2 Fig. 11b' both exhibiting similar etch figure shapes, depending on twinning angles. Fig. 11c shows dislocation etch pits of the polished lunar plagioclase at high magnification. Dislocations could be distinguished from tracks by their shape and by the random orientation of track directions as opposed to that of dislocations, which are also often polgonized and associated with twin boundaries.

Table 1

EMX ANALYSIS OF OLIVINES IN 12052,43,1,1

	WT % of Element			
AREA	#1	#2A	#2B	#3
Mg	20.97	19.53	19.53	18.97
Si	17.52	16.97	17.16	17.24
Fe	20.50	22.21	22.39	23.32
Mn	.21	.24	.26	.22
Co	.41	.46	.44	.44
Ti	.07	.08	.09	.09
Cr	.27	.22	.21	.21
O	39.63+	38.55+	38.83	38.80
Total	99.57	98.26	98.91	99.29

Adhesion Studies

Two successful fractures of 12052,43 were made at ultrahigh vacuum (10^{-9} to 10^{-10} torr). Attempts to measure touch contact adhesion between the segments revealed that the net adhesion force was less than that measureable by the system ($<10^{2}$ dynes). However, indications of electrostatic charging were observed (specifically in adherence of fragments to the metal pieces associated with the fractures, and particle-alignment changes as the rock fragments were brought toward contact). The observed behavior was similar to that of the Apollo 11 samples and terrestrial rocks, but the adhesion force was orders of magnitude lower than the adhesion force measured for various terrestrial minerals studied previously.

The smaller section from the first fracture of 12052,43 was mounted on the UHV rotary feedthrough of the Cartesian cross assembly for measuring electrostatic charge (Grossman, 1969). Basically, a chisel and anvil are disposed along a line perpendicular to the rotary feedthrough. A 630 μm electrometer probe wire penetrates a ground-plane which is parallel to the fractured face. This probe translates radially along the third Cartesian axis. The surface can be mapped either by measuring charge or more sensitively the current produced by scanning the surface at different rotation rates. The fracture direction was along one diagonal of the rectangular sample but the fracture face penetrated the surface in approximately a circular arc centered near the chisel penetration, Fig. 12. The net charge of this face was found to be positive from the positive/negative current peak pair found as the electrometer probe traversed this fracture edge. In addition, a second positively charged section was found near the center of the arc, at a point just above the fracture arc. The average charge density in this region

was estimated to be 5 x 10^6 charges/cm^2 which is five orders of magnitude less than that found with single crystal terrestrial rocks and at least a factor of 10 lower than course grained granite.

On raising the pressure in the vacuum chamber to atmospheric with air, the effect of gas adsorption was observed as a change in relative (current) peak heights. After exposure to the laboratory atmosphere for approximately one week and then pumping the sample to 10^{-9} torr, we found the charge had decreased irreversibly by a factor of 20, which was very near the detectivity limit of the system. The same sample was fractured a second time from the opposite direction and again the fracture plane penetrated the crystal surface, but this time as a straight edge. A negative/positive peak pair associated with the fracture edge was found at UHV, which remained stable while raising the pressure up to atmospheric with dry nitrogen and then repumping to 10^{-9} torr. The sample was then irradiated with UV light through a sapphire window and the charge decreased a factor of 30 below background in four hours.

DISCUSSION

The Apollo 12 rock 12052,43 is an olivine basalt, consisting mainly of plagioclase, pyroxenes, olivine, ilmenite, and a chromium-spinel in a glassy matrix. Single crystals of some species are as long as 1 mm and 0.5 mm wide. The pyroxenes and olivine are mostly equant, and sometimes rounded. The plagioclase occurs in long radial laths and as skeletal crystals, and ilmenite plates intersect the surface parallel to plagioclase laths. A band of ilmenite surrounding a chromium-spinel core was found. The rock is very porous, with

numerous craters lined with glass splashes and glass rims. Microfracturing or glassy deposits give the external surface a "sugary" effect. Single crystals, visible in the light microscope, exhibited deformation features such as bent twinning bands, fracturing, and displacement. Few spheres were visible on the surface but some were found embedded in the rock after sectioning.

The chemical etch-pit method was employed to reveal the processes that modified the structure of lunar rocks. The relative simplicity of the method, which allows study of the structure of bulk cleaved or polished crystals, and following the structure in depth by successive polishing/etching steps, has some advantage over, and compliments studies of the rocks by thin sectioning and transmission electron microscopy. Chemical etching brought out a variety of crystal structural features. These included twinning, banding, exsolution with twinning, growth bands, and skeletal structures. Deformation features, as kink bands, subgrain low angle tilt boundaries and microfracturing were also found. Dislocations and cosmic ray tracks (ratio 1:3 and less) have been found in pyroxenes, olivine, plagioclase and ilmenite in the interior of the 12052,43. Other mineral species present in the rock, such as apatite, crystobalite and others were not examined in detail.

The most interesting accomplishment of the microchemical study of the Apollo 11 and 12 lunar rocks was revealing both dislocations and fossil tracks in olivine, heavy cosmic ray tracks in pyroxenes and ilmenite and the variations in the pyroxene compositions, exhibited by etched striations in the high calcic augite. The etching results show that the lunar rocks examined were subject to deformation, melting and high temperature recrystallization, slow cooling

resulting in chemical differentiation and fractionation, and crystal structure damage from cosmic rays, fissionable compounds and meteoritic impacts.

In an attempt to assess the bonding, elemental analysis of the gas disrupted areas and their surroundings were made by electron microprobe. Besides the major elements, a search was made for those minor elements which are known to form hydrogen bonding or hydrides in the solid state, because it was thought that hydrogen atoms derived at the lunar surface from solar wind and solar cosmic ray protons might form hydrogen bonding in conjunction with these elements. There were no distinctive differences in elemental composition between the gas disrupted areas and their surroundings. Nevertheless, in some cases atomic bonding might still be present. If so, the contact areas for bonding of the gas disrupted particles are few and the linear dimension of each area is smaller than the 0.1 μm scale that can be seen by the magnification used in Fig. 3.

The net positive charge found on the UHV fractured face of lunar rock 12052,43 is expected from strain-free fracture of a homogeneous insulator with a positive electron work function. The probe and probe distance used are large compared to the average grain size and, therefore, averages out local inhomogeneous electric fields previously observed on Apollo 11 samples by the orientation effect on 100 μm and smaller particles. We conclude, therefore, that the lack of adhesion of fractured lunar rocks on a macroscopic scale is due both to the statistical local charge averaging to zero over the rough surface and the repulsive force produced by work function effects when creating a fresh surface in UHV.

A general conclusion is that samples returned by Apollo 11 and 12 missions are susceptible to disruption when exposed to oxygen and water vapor. When

the interior surface of the fractured rock was exposed to nitrogen, no change in the macroscopic charge distribution was observed. This can be used as direct evidence that the bulk properties of lunar rocks are not affected by processing in dry nitrogen. However, some surface properties, for example irreversible adsorption of the lunar fines, may be affected and require investigation in these special cases.

A discussion of electrostatic adhesion forces (greater than Van der Waals' forces) stabilized by solar ultraviolet irradiation was recently presented (Grossman, 1970). Briefly, disturbed lunar soil particles which randomly contact new particles will undergo induced photoelectric and photoconductive charge redistribution until a steady state charge distribution is established. The average thickness of the charged layer (the Debye length) and, therefore, the force of adhesion depends on the particle work functions, solar flux, the temperature, the UV adsorption coefficients, the dielectric constants and the conductivity. Preliminary results (Gupta, 1970) suggest that lunar material solar cosmic ray damaged surfaces have higher conductivity than terrestrial particles. We conclude tentatively that the unusual cohesive properties of lunar soil are due to a combination of electrostatic effects all attributable directly to the absence of a lunar atmosphere.

Acknowledgments--We specially thank W. M. Hansen, A. D. Pinkul, E. L. Miller, A. Phillips, and Mrs. B. Tooper for their contributions to the program. This work was supported by NASA Contract NAS9-8082.

REFERENCES

Barber, D. J., Hutcheon, I., Price, P. B., (1971). Extralunar Dust in Apollo Cones, Science, 171, 372-374.

Belov, N. V., Acad., 1965. Crystal Structure of Large Cation Silicates, Transl. Consultants Bureau, New York.

Condie, K. C., Kuo, C. S., Walker, R. M., Murthy, R. V., (1969). Uranium Distribution in Separated Clinopyroxenes from Four Eclogites, Science, 165, 57.

Fleischer, R. L., Price, P. B., Walker, R. M., Maurette, M., (1967). Origins of Fossil Charged-Particle Tracks in Meteorites, J. Geophys. Res., 72, 331-353.

Fleischer, R. L., Haines, E. L., Hanneman, R. E., Hart, H. R. Jr., Kasper, J. S., Lifshin, E., Woods, R. T., Price, P. B., (1970a). Particle Track, X-ray, Thermal, and Mass Spectrometric Studies of Lunar Materials, Science, 167, 563-571.

Fleischer, R. L., Haines, E. L., Hart, Jr., H. R., Woods, R. T., and Comstock, G. M., (1970b). The Particle Track Record of the Sea of Tranquility, Proc. Apollo 11 Lunar Sci. Conf., Geochim. Cosmochem. Acta Suppl. 1, Vol. 3, 2103-2120. Pergamon.

Grossman, J. J., (1969). Electrostatic Charge Distribution on Ultrahigh Vacuum Cleaved Silicates, J. Vac. Sci. Tech., 6, 233-236.

Grossman, J. J., Ryan, J. A., Wegner, M. W., (1970a). Experimental Investi-

gation of Ultrahigh Vacuum Adhesion as Related to the Lunar Surface, Final Contract Report, Fifth Year Summary, 1 Jan. 1969 through 19 June 1970, NAS7-307.

Grossman, J. J., Ryan, J. A., Mukherjee, N. R., Wegner, M. W., (1970b). Microchemical, Microphysical, and Adhesive Properties of Lunar Material, Proc. Apollo 11 Lunar Sci. Conf. Geochim. Cosmochim. Acta Suppl. 1, Vol. 3, 2171-2181. Pergamon.

Grossman, J. J., (1970). Lunar Soil Adhesion Due to Electrostatic Forces Stabilized by Solar Radiation, Trans. Am. Geophys. Union, 51, 772.

Gupta, Y. P., (1970), Private Communication.

Lunatic Asylum, (1970), Mineralogic and Isotropic Investigations on Lunar Rock 12013, Earth and Planet. Sci. Letters, 9, 137-163.

Maurette, M., (1966). Etude des traces d'ions lourds doris les mineraux naturels d'origine terrestre et extra-terrestre. Bull. Soc. Franc. Miner. Crist. 89., 41-79.

Wegner, M. W., Grossman, J. J., (1969). Dislocation Etching of Naturally Deformed Olivine, Trans. Amer. Geophys. Union, 50, 676.

Young, C. III (1966). Applications of Dislocation Theory to Upper-Mantle Deformation. Ph.D. Disseration, Stanford University.

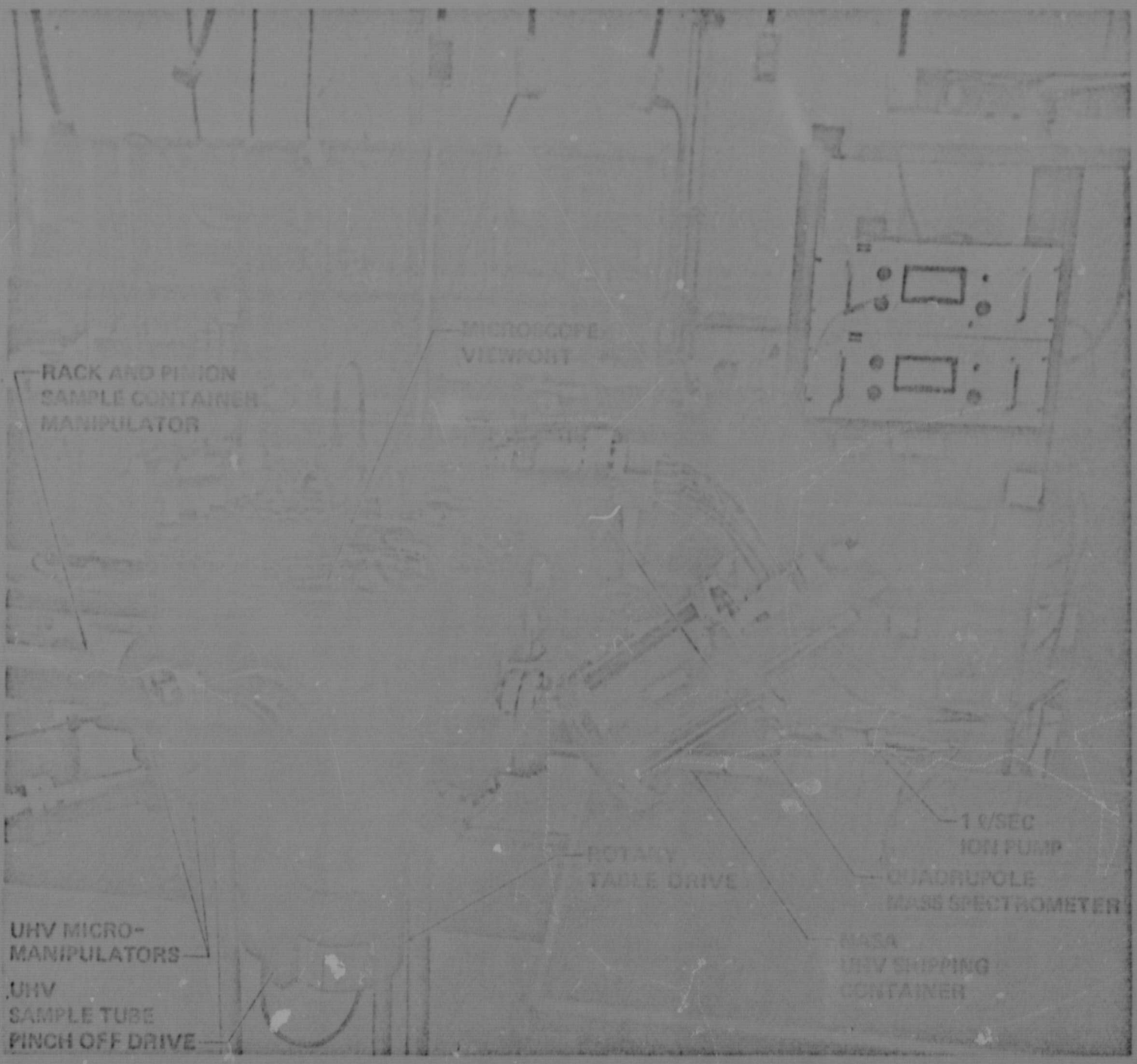

Figure 1. NASA Vacuum Pumped Shipping and Storage Container Connected to MDAC-West UHV Micromanipulator Chamber. The Container is Closed, Storing the Remainder of Lunar Samples 12001,118 After Vacuum Transferring a Part of the Sample to Gas Exposure Cells

Figure 2. Scanning Electron Micrograph (From Stereo Pair) Viewed Normal to Bonding Plane of Two Disrupted Crystals, One Right of Center Over Horseshoe Area and the Second Above this Area and Further to the Right. Arrows Point to Examples of Deposits Attributed to Liquid Spray. (See Figure 2a, Grossman et al. 1970a)

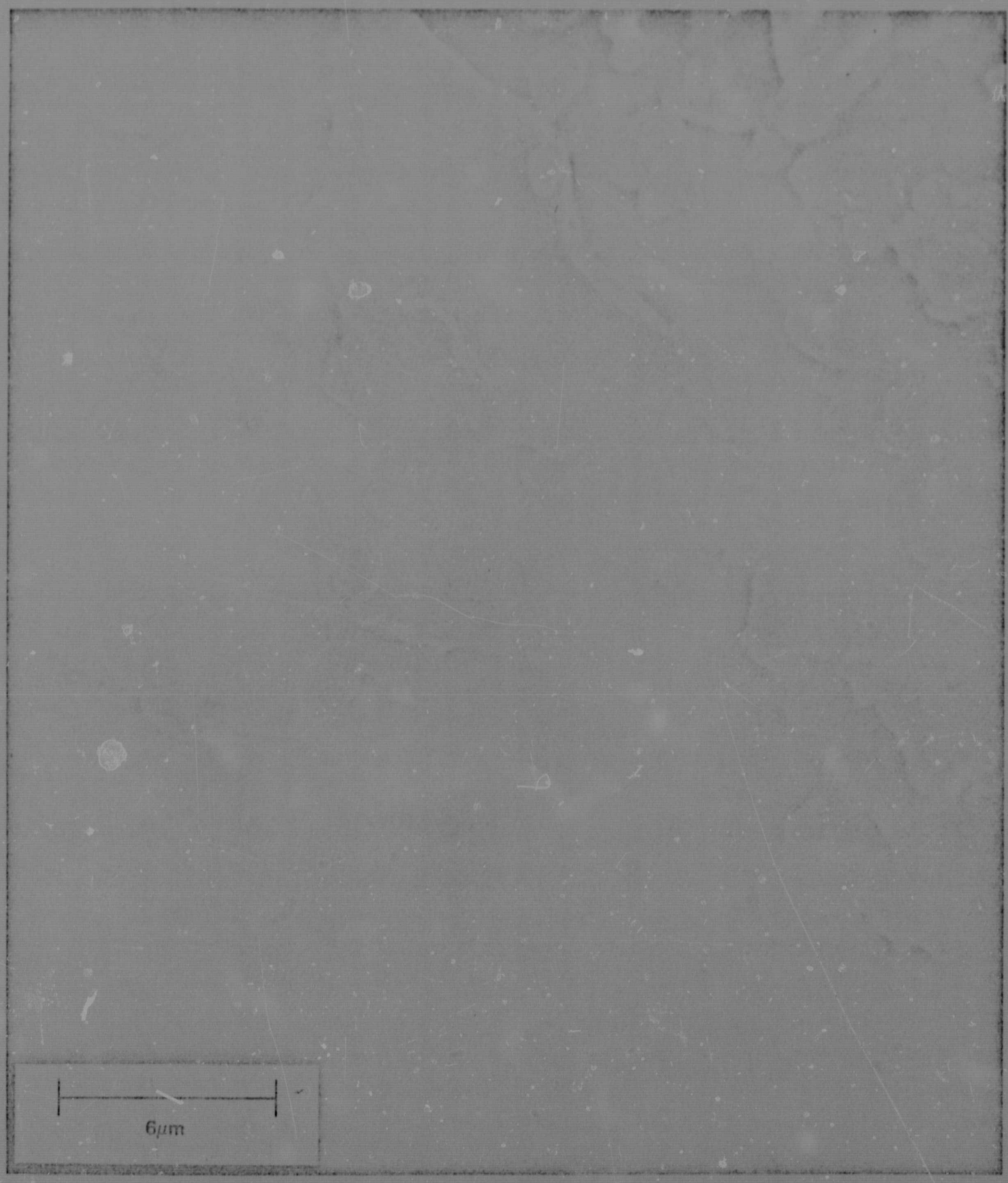

Figure 3. Scanning Electron Micrograph Viewed 30 Degrees From Normal of Plane From Which Rice Grain Shaped Crystal Disrupted (See Figure 2c, Grossman et al. 1970b). The Crystal was Adhering in an end on Position in the Cavity in the Lower Central Region of the Photomicrograph

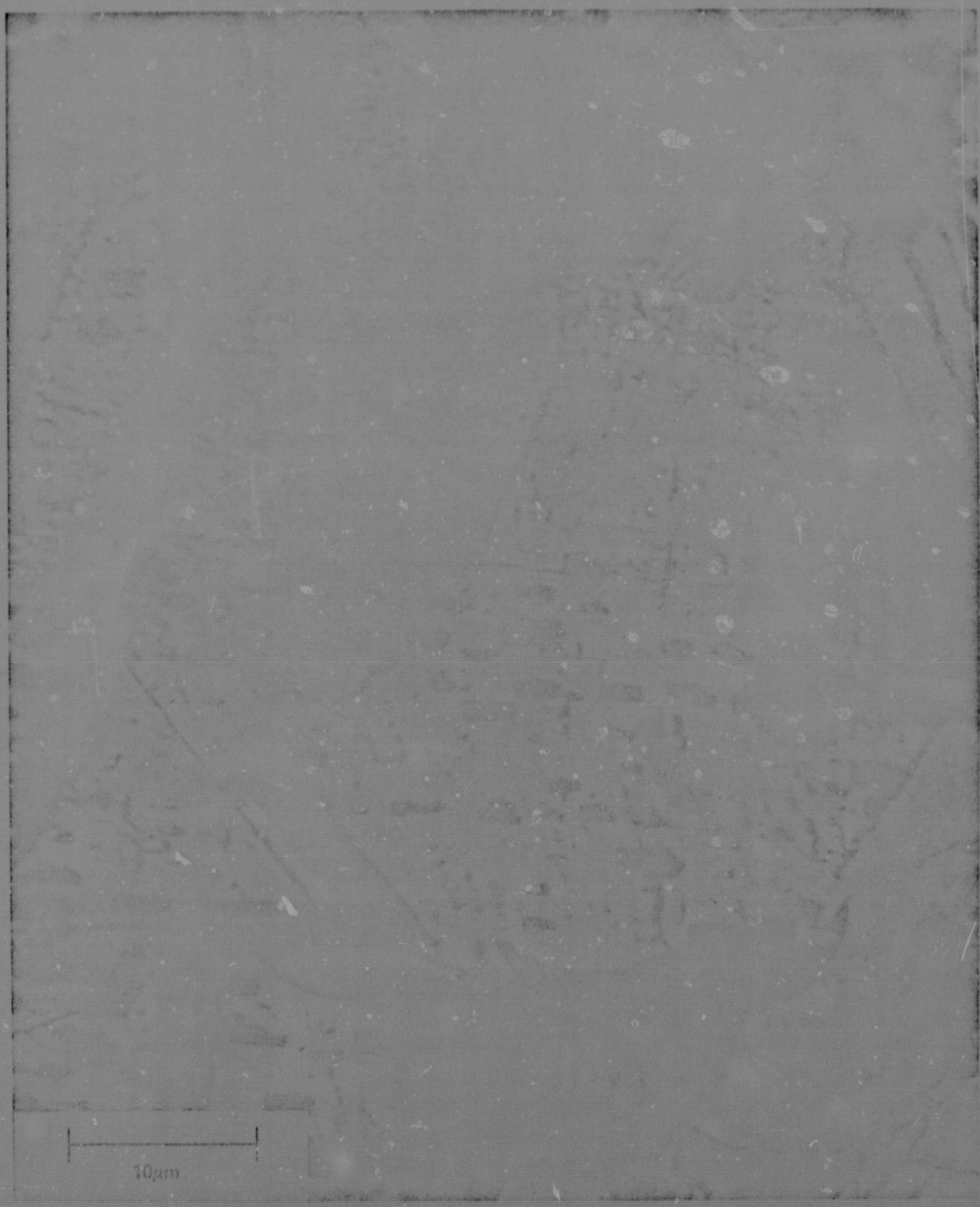

Figure 4. Dislocation Etch Pits and Tracks in Olivine (12052,43,2)

Figure 5. Cosmic Ray Tracks in Pyroxene (Dots) (12052,43,2)

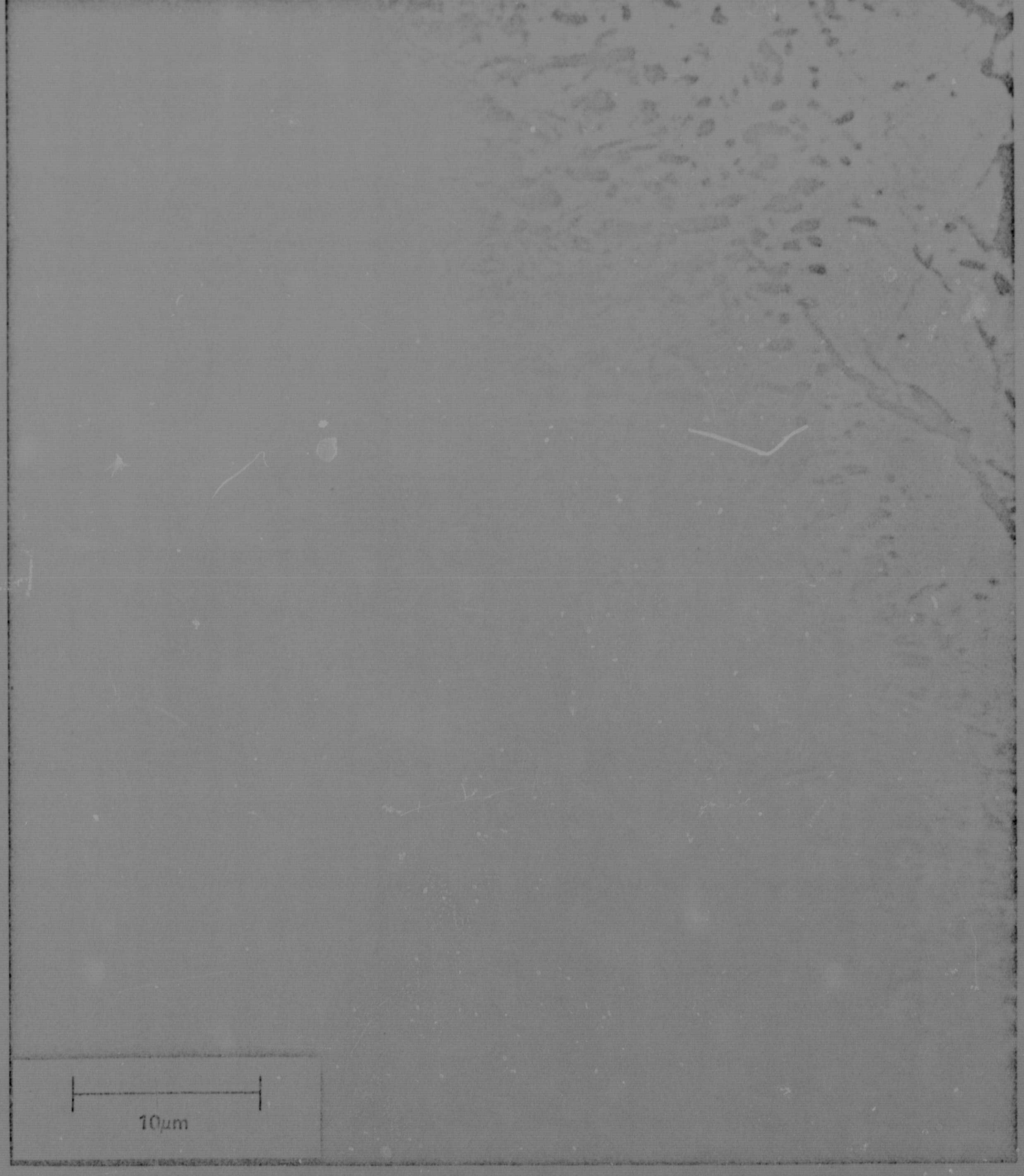

Figure 6. Heavy Cosmic Ray Tracks in Edge of Pyroxene Crystal (12052,43,2)

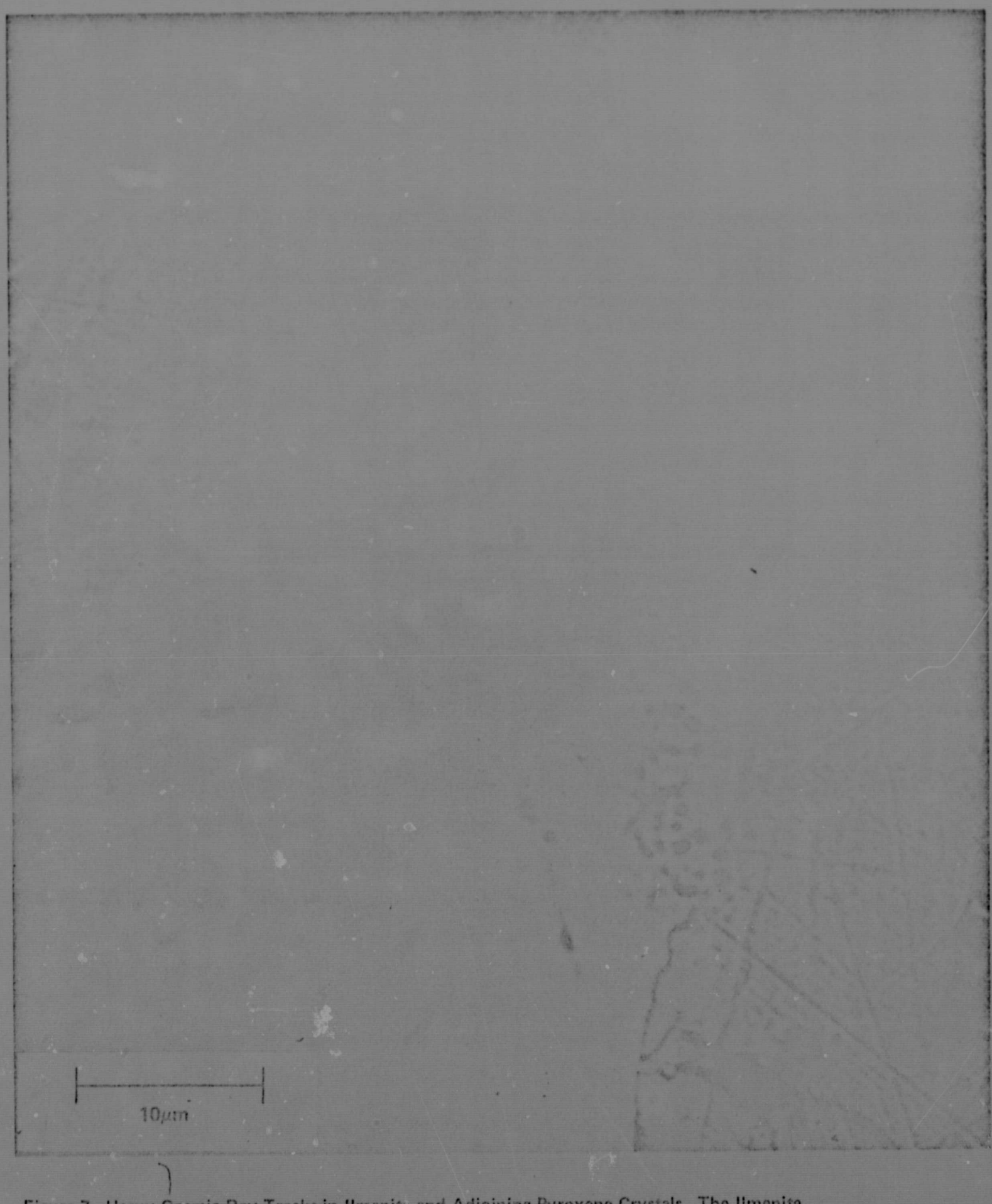

Figure 7. Heavy Cosmic Ray Tracks in Ilmenite and Adjoining Pyroxene Crystals. The Ilmenite Borders an Unetched Chromite Crystal (12052,43,2)

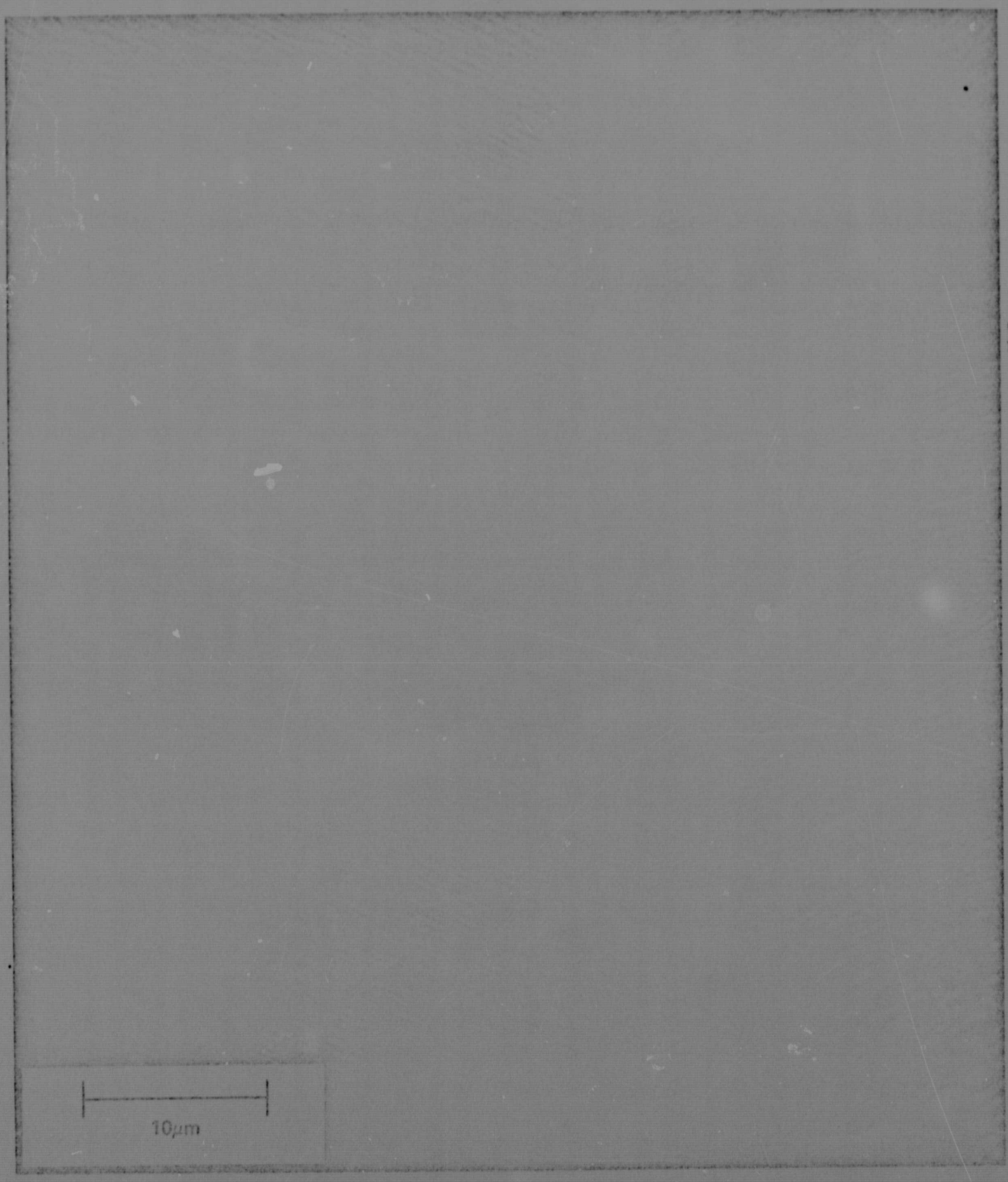

Figure 8. Etched Striations in High Calcic Phase of Pyroxene Crystal (12052,43,2)

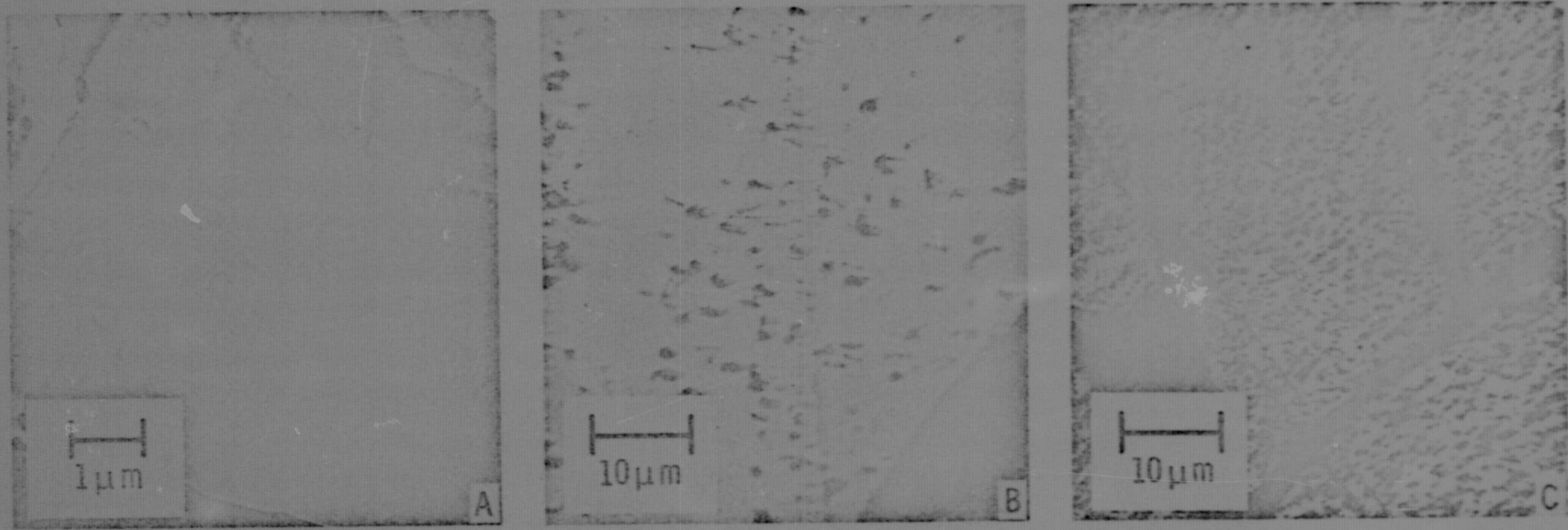

Figure 9. Dislocation Etch Pits and Tracks in Polished Olivine Crystals. Approximate Orientations are: (a) (100) Face; (b) (010) Face; (c) (001) Face (12052,43,1,1)

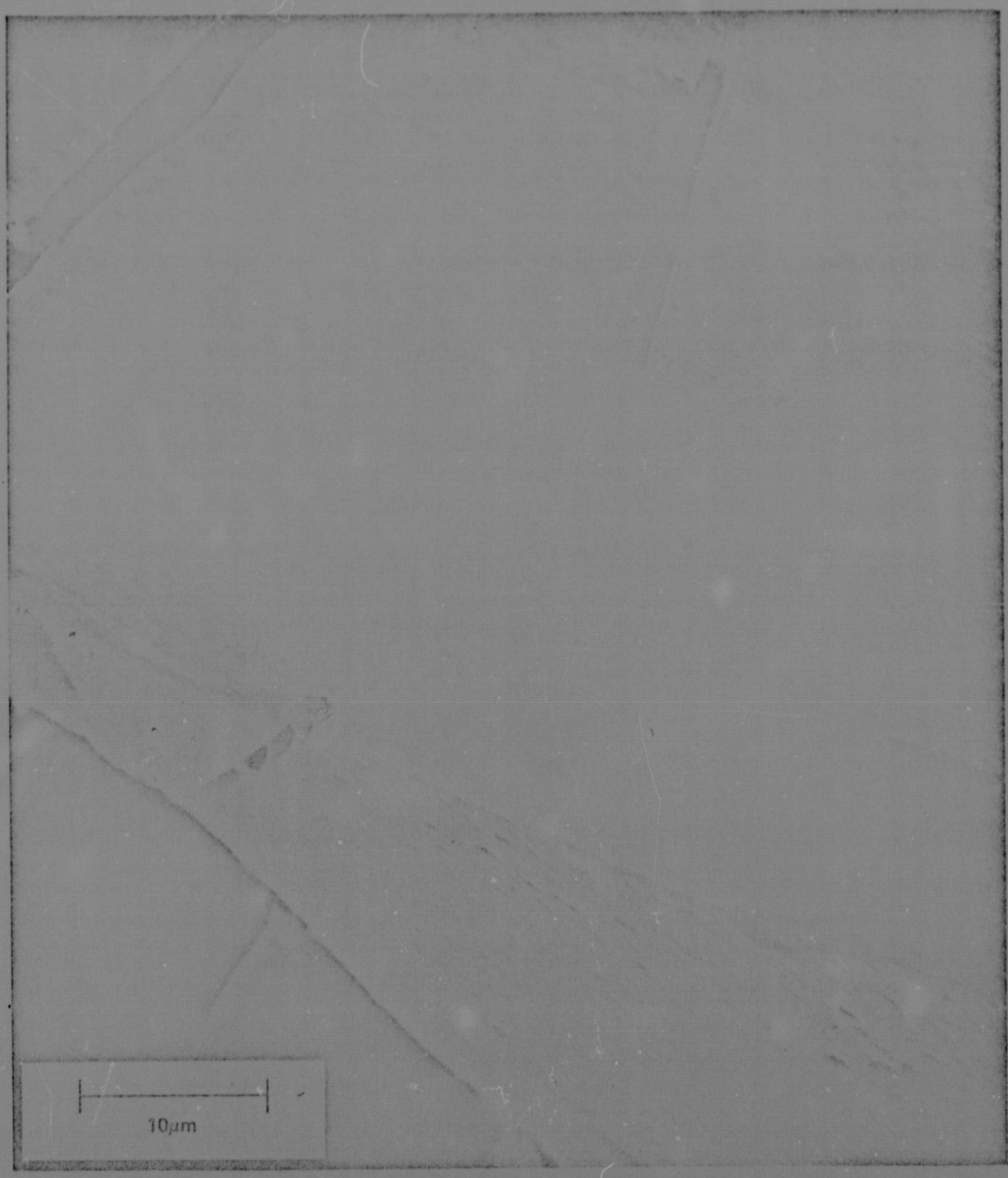

Figure 10. Microcracks at Interface of Olivine Crystal and Ilmenite Inclusion (12052,43,1,1)

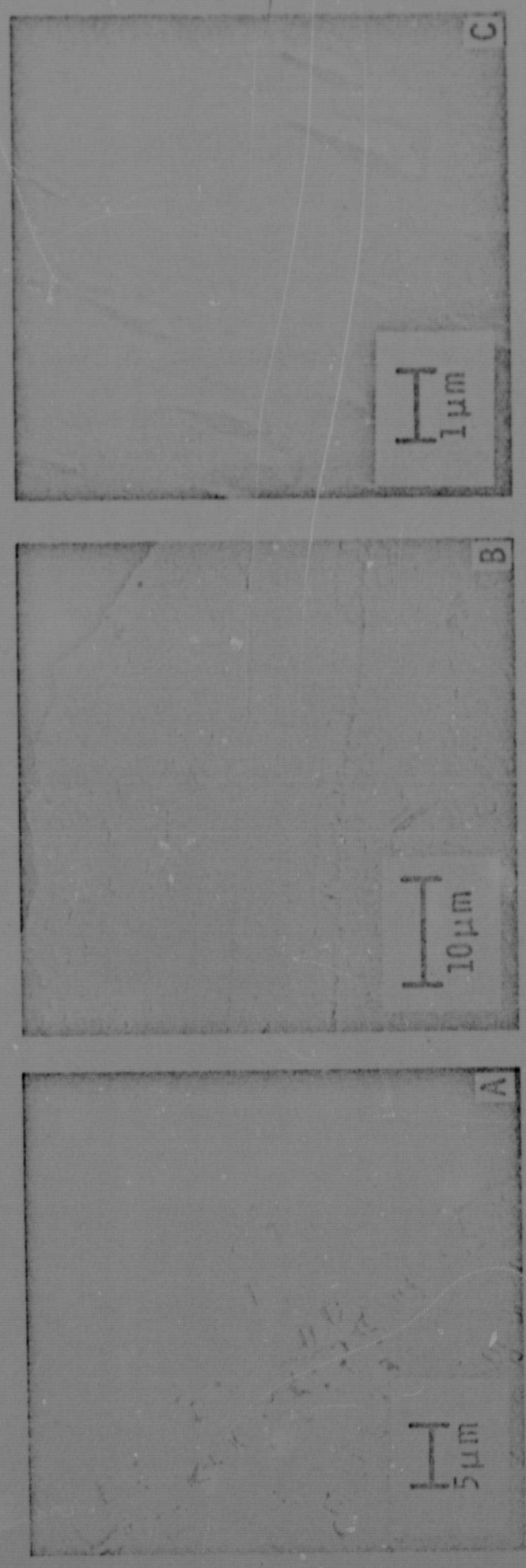

Figure 11. Dislocation Etch Pits and Twin Boundaries in (a) Madagascar Albite, Cleaved (001), and (b, c) Polished Lunar Plagioclase (10053,40,2)

Figure 12. Fracture Face of Lunar Sample 12052,43,1,2,1,1 After Measuring the Electrostatic Charge Distribution. The Specimen is Approximately 5 mm Wide. Present Orientation is approximately a 150 Degree Clockwise Rotation from Fracture Position